Non-uniform ramping losses and thermal optimization with turn-to-turn resistivity grading in a (RE)$Ba_2Cu_3O_x$ magnet consisting of multiple no-insulation pancake coils

Yawei Wang,[1,2)] Min Zhang,[1)] Weijia Yuan,[1)] Zhiyong Hong,[2)] Zhijian Jin,[2)] and Honghai Song,[3,a)]

[1]*Departmentof Electronic and Electrical Engineering, University of Bath, BA27AY, Bath, UK*

[2]*Department of Electrical Engineering, Shanghai Jiao Tong University, 200240, Shanghai, China*

[3]*Brookhaven National Laboratory, Upton, NY, 11973, USA,*

This paper presents a study on the ramping losses of a high temperature superconductor (HTS) magnet consisting of multiple no-insulation (NI) (RE)$Ba_2Cu_3O_x$ coils. The (RE)$Ba_2Cu_3O_x$ (REBCO) conductor is the second generation HTS thin tape where RE stands for rare-earth. During a ramping operation of the NI HTS magnet, Losses are generated both across turn-to-turn resistances and inside superconducting layers. The former comes with radial current, which is called 'turn-to-turn loss'; the latter one is induced by flux creep and jump, called 'magnetization loss'. The modeling and experimental studies on the ramping losses have been reported on a single NI pancake coils in the previous part. In a HTS magnet consisting of multiple NI coils, the electromagnetic coupling between coils have a considerable influence on the distribution of ramping losses. Here the experimentally validated model is used to investigate a HTS magnet consisting of 14 single pancake (SP) REBCO coils. Results show that both the turn-to-turn loss and magnetization loss present a significant non-uniform distribution among coils. The highest turn-to-turn loss occurs to the middle coils of the magnet, while the highest magnetization loss happens on the end coils. The non-uniform distribution of ramping losses can result in a considerable temperature difference among coils in the NI HTS magnet. It leads to an additional quench risk on the magnet and requires more attentions in design. The distribution of the turn-to-to-turn loss can be optimized by adjusting the turn-to-turn resistivity. A much more uniform turn-to-turn loss distribution among coils is achieved by applying a graded turn-to-turn resistivity on the multiple coils.

I. INTRODUCTION

The no-Insulation (NI) high temperature superconductor (HTS) coil is wound directly with bare HTS tapes, and does not have traditional turn-to-turn electrical insulation [1-3]. As a result, in superconducting state, the current flowing circularly in azimuthal direction maintaining the magnetic field and storing magnetic energy, but the current may be directly bypassed through neighboring turns when local quench occurs. The local hot spot immedicably spread out in radial direction out and it prevents from local overheating and damage. Thus it provides a natural protection and potentially solves the challenging HTS quench degradation issue[4]. Compared to its insulated counterpart, the NI HTS coil shows an enhanced thermal stability during quench operations, which are of great interests and potentials for DC magnet applications, such as high field magnet, DC induction heater and MRI/NMR [5-13]. The Joule loss generated inside coils is a critical issue in charging of HTS magnets, which is called 'ramping losses' in this study. The temperature rise beyond threshold induced by the ramping losses is often the main cause of a ramp failure [14-16]. With such a considerable heat load, the total ramping losses has to be accurately estimated in the system cryogenic design. In conventional insulated HTS coils employing Kapton or Mylar, this ramping losses inside coils is

Electronic Email: y.wang2@bath.ac.uk and HonSong@bnl.gov

induced by flux creep in superconducting layer when the transport current is lower than the critical current[17, 18]. It is called 'magnetization loss' in this study. In NI HTS coils, an additional Joule loss is generated by radial current between turns, due to the absence of turn-to-turn electrical insulation. It is called 'turn-to-turn loss' in this study[19].

The ramping losses of traditional insulated HTS magnets have been studied in detail in experiments and with modeling [14-16, 20, 21]. Researches on the ramping behaviors of NI HTS coils have been performed with regards to voltage and current by modeling and experiments[22-30]. Regarding the ramping losses, a study on single pancake NI HTS coils has been conducted in our recent report. Therein, an experimentally validated model is proposed to calculate the ramping turn-to-turn loss and magnetization loss in the NI HTS coil [19]. However, in industry applications, the HTS magnet usually consists of multiple coils [5, 6, 31-40]. The distribution of ramping losses on a multiple NI coil system is most likely be affected considerably by the complexity electromagnetic coupling among coils and resulted non-uniform current distribution [41]. A 26 T all-REBCO magnet has been built with 26 NI pancake coils in 2015 [33]. During the ramping test of this magnet, the current ramp has been interrupted several times because of the temperature rise induced by ramping losses. As a result, such ramping losses of the multiple NI coil system become a very practical problem for the application of NI technique.

Continue our recent study in ref [19], this paper plans to study the ramping losses of a HTS magnet with multiple NI coils, as a sister paper. A HTS magnet is designed with 14 identical NI single pancake (SP) coils. The experimentally validated model for the calculation of ramping losses in previous report is expanded to multiple NI HTS coil system. A heat transfer model is coupled to calculate the temperature rise induced by the ramping losses. The ramping losses including turn-to-turn loss and magnetization loss of the 14 NI coils system are calculated using the multiple physics model. Losses of the NI HTS magnet and its insulated counterpart are compared. Temperature rise owing to the ramping losses is analyzed and the weak point of the multiple NI coil system is localized and discussed. A considerable non-uniform distribution of ramping losses among coils is discovered and a graded turn-to-turn resistivity method is proposed to uniform the loss distribution and optimize thermal difference among coils.

II. A HTS MAGNET CONSITING OF MULTIPLE NI REBCO COILS

A NI HTS magnet with 14 identical SP coils connected in series is investigated. The coils are numbered SPC1~SPC14 from the bottom to the top, as shown in Fig. 1. Each coil has 100 turns and the turns in each coil is numbered 1~100 from the inner side to the outer side of the coil. The initial operational temperature of the magnet is 20 K. The coil is wound by REBCO tapes from Superpower, USA. The width and thickness of each turn are 4 mm and 0.2 mm respectively. The inner/outer diameter of the coil is 100/140 mm, and the distance between adjacent coils is 2 mm. The equivalent turn-to-turn resistivity of the NI coil is 70 μΩ·cm^2. More detail about this magnet is shown in Table 1.

The field dependent critical current in (4) is calculated[42] as:

$$I_c(B,\theta) = I_c(B_{par}, B_{per}) = \frac{I_{c0}(T)}{[1+\sqrt{(kB_{par})^2 + B_{per}^2}\,/\,B_c]^b} \tag{1}$$

where I_{c0} is the critical current in self-field, B_{par} and B_{per} are the magnetic field parallel and perpendicular to the tape surface respectively. k, b, B_c can be obtained by fitting measurement data, whose values are 0.063, 1.46, 4.14 respectively for the REBCO tape in this study.

The temperature dependent critical current I_c in (4) is calculated [43, 44] as:

$$I_{c0}(T)=\begin{cases} I_o\left(\dfrac{T_c-T}{T_c-T_o}\right)^{1.3} & if\ T<T_c \\ 0 & if\ T\geq T_c \end{cases} \tag{2}$$

where T_o= 77 K, I_o=100 A is the self-field critical current at 77 K, T_c= 92 K is the critical temperature. The critical current of the magnet is 330 A at 20 K, and the operating current is set to be 200 A. The critical temperature of the magnet T_{cs} at this operating current is 52 K, at which the critical current of the magnet is equal to the operating current 200 A.

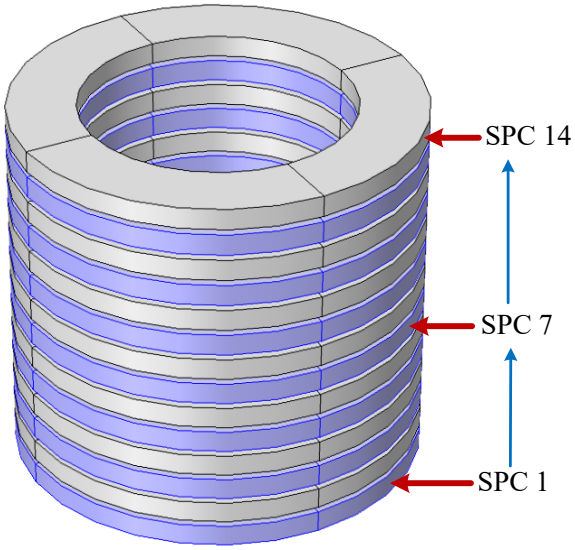

FIG. 1. Schematic illustration of the HTS magnet with multiple NI REBCO coils.

TABLE I. Specifications of the NI HTS magnet investigated.

Parameters	Magnet
Type of the coil	Single pancake
Number of turns, each SP coil	100
Inner/outer diameter, SP coil	100/140 mm
Height of the magnet	82 mm
B_z per amp, at magnet center	11.7 mT/A
Magnet self-inductance, L_m	177 mH
I_c, magnet	330 A @ 20 K
Turn-to-turn resistivity	70 μΩ·cm^2

III. A HYBRID NUMERICAL MODEL

During the ramping operation of the NI HTS magnet, transport current from power supply flows along the azimuthal and radial direction. The radial current generates the turn-to-turn loss on contact resistances. The azimuthal current flows in superconducting layers below critical temperature and generates a transport loss in superconducting layers, which is so-called magnetization loss[19]. These losses will result in a temperature rise across each coil and among the coils, and even variation of

local critical current. Overall, all these will have an effect on the magnetization loss in superconducting layers. An experimentally validated numerical model has been proposed to calculate the ramping turn-to-turn loss and magnetization loss of a single NI REBCO coils in previous report [19]. Here it is expanded on multiple NI REBCO coil system, and a heat transfer model is coupled to calculate the temperature rise induced by the ramping losses.

A. Calculation of ramping turn-to-turn loss and magnetization loss

The ramping losses of NI coils are calculated by a numerical model coupling an equivalent circuit network model and an H-formulation HTS model. The equivalent circuit network model is to calculate the distribution of the azimuthal current and radial current on the NI coil. In this model, each turn of the coil is subdivided into fine arc elements, each arc element is equivalent to lumped circuit parameters, and each SP NI coil is equivalent to a circuit network, as shown in Fig. 2(a). Therefore the whole NI HTS magnet is equivalent to 14 circuit networks in series [28, 45]. The governing equation of this model is derived from Kirchhoff's current and voltage laws. The turn-to-turn loss can be obtained directly from this model:

$$\begin{cases} W_{t2t} = \sum_k {j_k}^2 R_k \\ Q_{t2t} = \int W_{t2t} dt \end{cases} \tag{3}$$

where j_k and R_k represent the radial current and the equivalent turn-to-turn resistance of the k-th arc element. W_{t2t} and Q_{t2t} are the turn-to-turn loss power and energy respectively. This model has been validated experimentally in previous publications [19, 28]

The electromagnetic model based on H-formulation is to calculate the magnetization loss in superconducting layers. It is coupled to the above equivalent circuit network model. The current distribution from the circuit network model is inputted into the electromagnetic model, and it is imposed on the domain of each turn. Since both the azimuthal and radial currents show uniform distribution along angular direction on most turns of the NI coil, the physical 3D object can be simplified to a 2D axisymmetric model. Considering the symmetry along the axial direction of the magnet, only the upper 7 SP coils are solved in this model, as shown in Fig. 2(b). The magnetization loss in superconducting layers is calculated by:

$$\begin{cases} W_{sc} = \int_\Omega \mathbf{E} \cdot \mathbf{J} \mathrm{d}\Omega \\ Q_{sc} = \int W_{sc}(t) \mathrm{dt} \end{cases} \tag{4}$$

where W_{sc} and Q_{sc} are the magnetization loss power and energy respectively. **E** and **J** represent the electrical field and current density respectively. This model is solved by a commercial finite-element software, Comsol Multiphysics™. The coils on the ends of the magnets are meshed finer than others, because of more flux penetration on these domains.

This model shows an accurate estimation on the ramping losses of NI REBCO coils, which has been validated experimentally in previous report [19].

B. The embedded thermal model

The thermal model is to calculate the temperature changes caused by the total ramping losses. The turn-to-turn loss and magnetization loss from the above two models is input into the thermal model as heat source. The temperature rise obtained from this model is input into the electromagnetic model to update the critical current of REBCO tapes. The governing equation of this model is:

$$dC_p \frac{\partial T}{\partial t} + \nabla \cdot (-k \nabla T) = Q_{t2t} + Q_{sc} \tag{5}$$

where d and C_p are the density and heat capacity, Q_{sc} and Q_{t2t} are magnetization loss and turn-to-turn loss respectively. A homogenous heat parameters (thermal conductivity and heat capacity) are used for the REBCO tape, which neglect the temperature difference along the width and thickness direction of the REBCO tapes. Since both the turn-to-turn loss and magnetization loss show a uniform distribution among angular direction, the thermal model is built as a 2D axisymmetric model, which has a same geometry with the above electromagnetic model, as shown in Fig. 2(b). Two cooling conditions are analyzed in this study: perfect cooling with no temperature rise induced and adiabatic condition without any cooling.

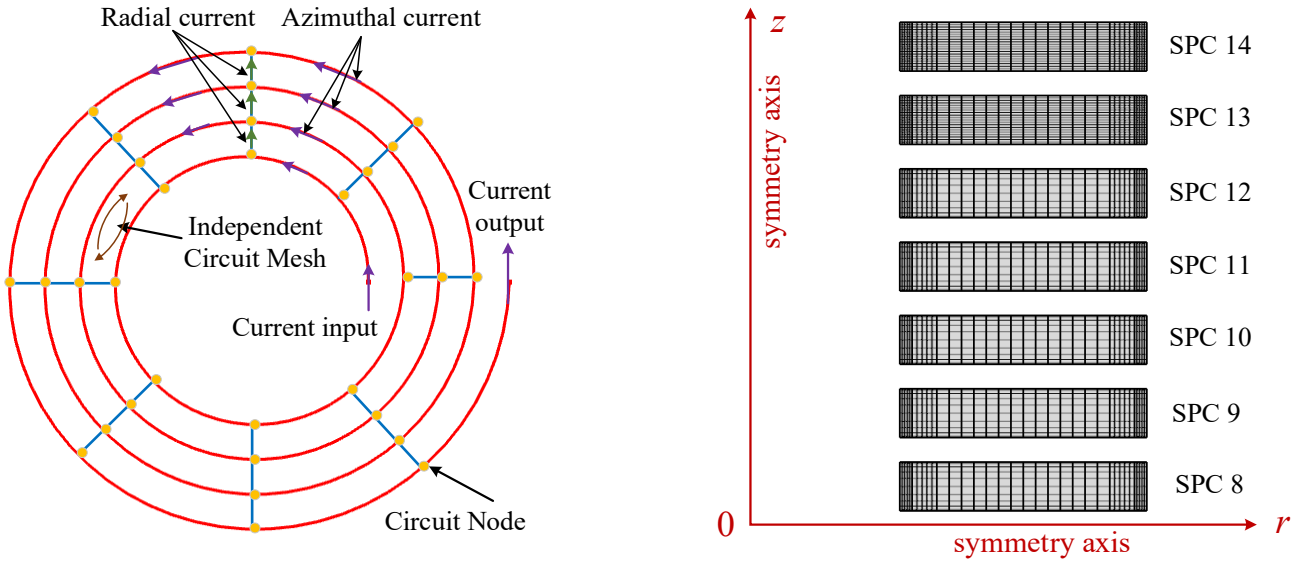

(a) Equivalent circuit network model

(b) FEM model
(EM model and thermal model)

FIG. 2. The hybrid numerical model used to calculate the ramping losses of multiple NI REBCO coil system.

IV. SIMULATION RESULTS

The HTS magnet with 14 NI coils are ramped up to 200 A in series with a ramping rate of 5 A/s, then the current of power supply is kept at the target current 200 A. Note that the ramping rate is that of the transport current from power supply, it is higher than that of the real ramping rate of azimuthal current in NI HTS coils. The ramping turn-to-turn loss and magnetization loss generated in this ramping process are calculated using the above hybrid numerical model. Also note that the ramping rate 5 A/s is a relatively higher ramping rate for both traditional low T_c superconductor and the high T_c superconductor. It has been chosen for the worse-case scenario analysis regarding ramping losses and thermal behaviors.

A. Distribution of the turn-to-turn loss

With a perfect cooling condition, Fig. 3 shows the turn-to-turn loss power W_{t2t} on each NI HTS coil. Since the coils on the lower half-section (SPC7~SPC1) has symmetric turn-to-turn loss distribution with the upper ones (SPC8~SPC14), only upper half-section is presented in the figure. The results show that the turn-to-turn loss power increases with the transport current from power supply and reaches a peak point when the transport current stops increasing at the target value (t=200 s). Then the turn-to-turn loss power drops to zero gradually. The results also indicate that the NI coils on the middle part of the magnet have a higher turn-to-turn loss power W_{t2t} than that on the ends. Integrating the turn-to-turn loss power W_{t2t} over ramping time, Fig.

4 shows the distribution of the total turn-to-turn loss energy Q_{t2t} density in the whole ramping process. It shows a significant non-uniform loss distribution among coils. In each NI coil, the turns near the outer side have a higher turn-to-turn loss energy Q_{t2t} density than the turns near the inner side. Along the axial direction of the magnet, the turns on the middle part have a higher turn-to-turn loss energy density than that those on the ends. The highest turn-to-turn loss energy density (on the 80th turns of SPC7 and SPC8) is 3.71 times of the lowest one (on the 1st turn of the SPC 1 and SPC 14).

Note that this is a theoretical study on the fundamental characteristics of the ramping turn-to-turn loss and magnetization loss in a multiple NI HTS coil system. The ramping turn-to-turn loss may be reduced considerably by decreasing the ramping rate or increasing the turn-to-turn contact resistivity as reported in our recent publications[19, 34]. Therefore, lower ramping rate and higher turn-to-turn contact resistivity will be applied in a practical ramping operation regarding to the cooling power.

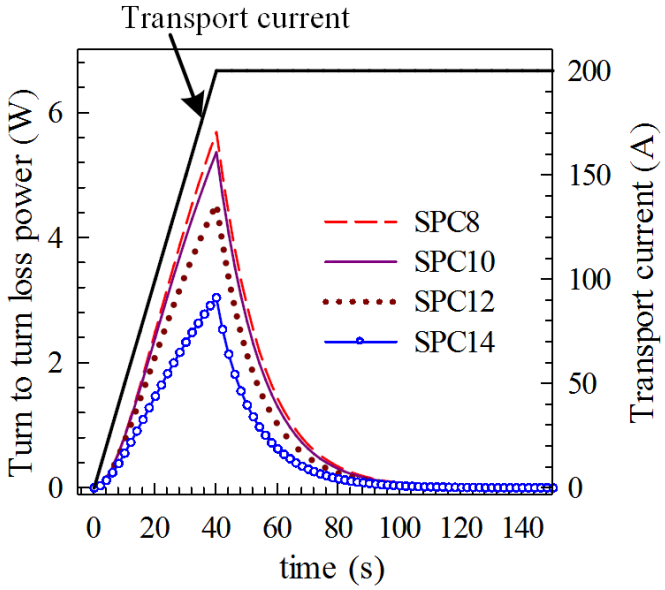

FIG. 3. The transport current and turn-to-turn losses power on each NI SP coil in the ramping process, perfect cooling condition, ramping rate 5A/s.

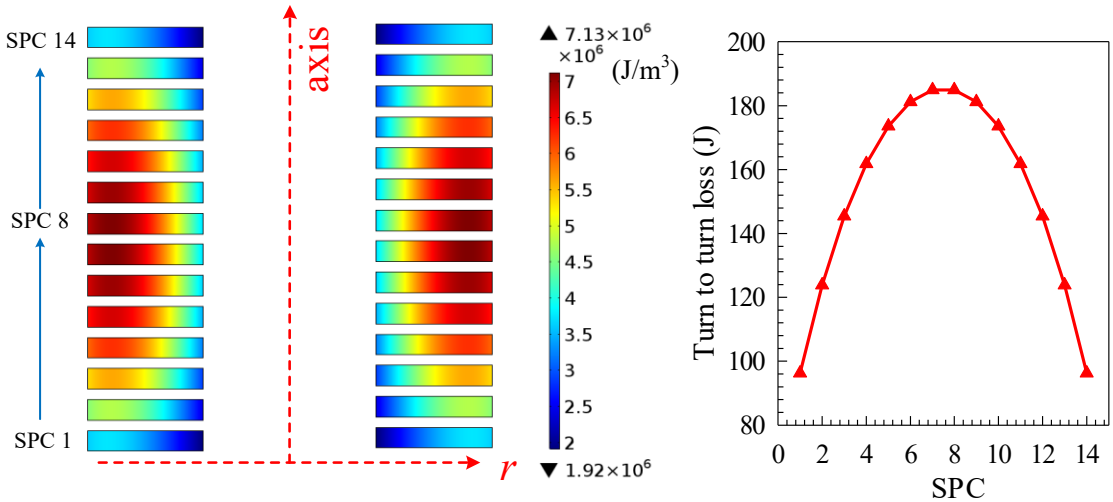

(a) Turn-to-turn loss energy density among turns

(b) Turn-to-turn loss energy among coils

FIG. 4. The total turn-to-turn loss energy generated in the whole ramping process with ramping rate 5A/s.

Since the turn-to-turn loss is generated by the radial current, its non-uniform distribution results from the current distribution. Fig. 5 shows the distribution of average radial and azimuthal current among turns in this ramping process. The average radial current of the m^{th} turn $I_{r,m}$ is the sum of radial current flowing through this turn, the average azimuthal current of the m^{th} turn $I_{s,m}$ is the average value of all the azimuthal current on this turn's arc elements. They are calculated from following formula:

$$\begin{cases} I_{r,m} = \sum_k j_{k,m} \\ I_{s,m} = \sum_k i_{k,m} \Big/ n_e \end{cases} \tag{6}$$

where $j_{k,m}$ and $i_{k,m}$ are the radial and azimuthal currents on k^{th} arc element of the *m-th* turn, n_e is the number of arc element on each turn. The radial current shows a similar distributions to the turn-to-turn loss. The azimuthal current shows an opposite distribution to the radial current, which is induced by the constraint of Kirchhoff's current law. The more transport current flows along the radial direction, the less current flows along azimuthal direction. The results validate that the distribution of the turn-to-turn loss is determined by the radial current, and the turns with higher radial current generates more turn-to-turn loss. The non-uniform distribution of the radial current is induced by the unbalanced electromagnetic coupling among turns. Fig. 6 shows the mutual inductance between different coils, the data on the diagonal is the self-inductance of each SP coil. SPC8's mutual inductances with others are considerably different than that of SPC14.

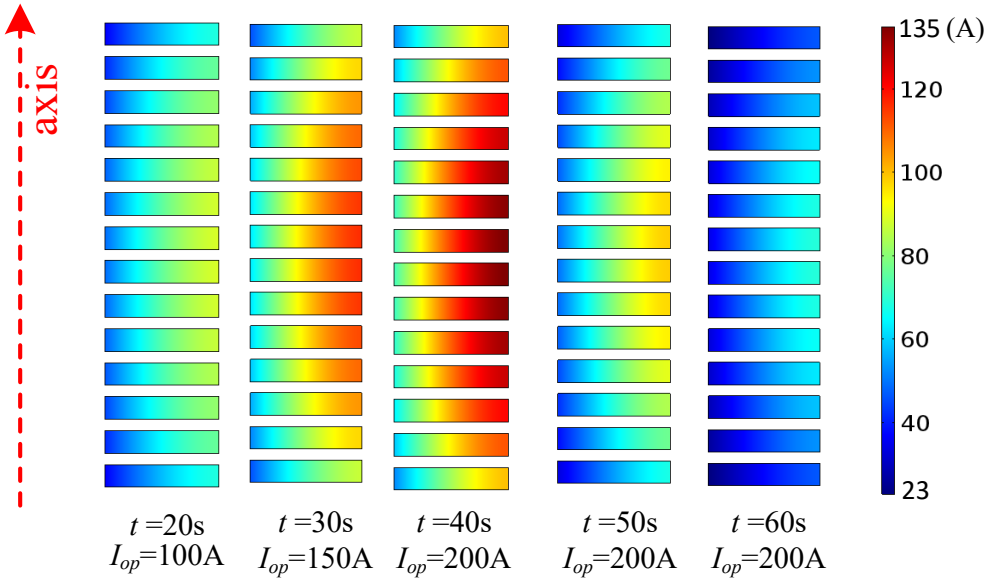

(a) Radial current

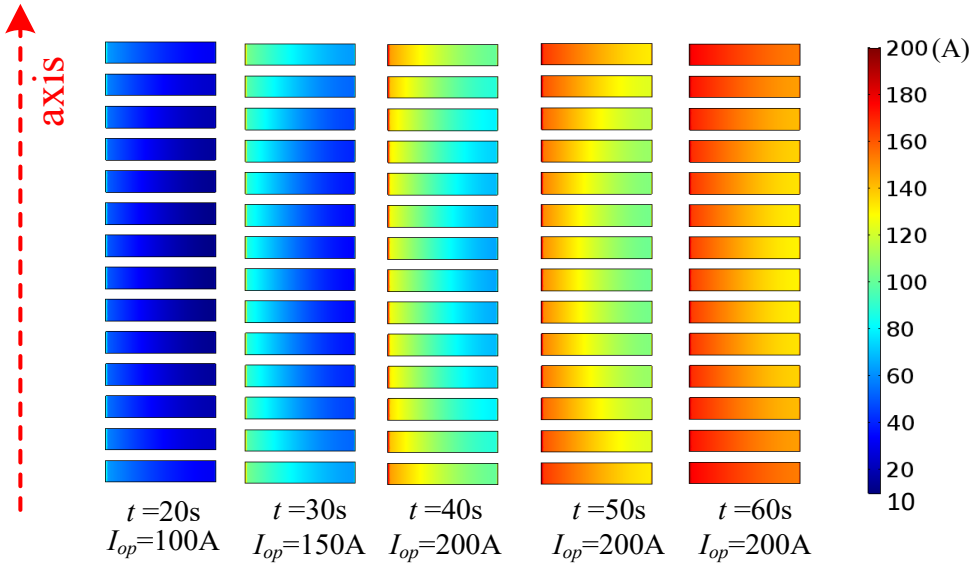

(b) Azimuthal current.

FIG. 5. The average radial and azimuthal current on each turn of the NI magnet in the ramping process.

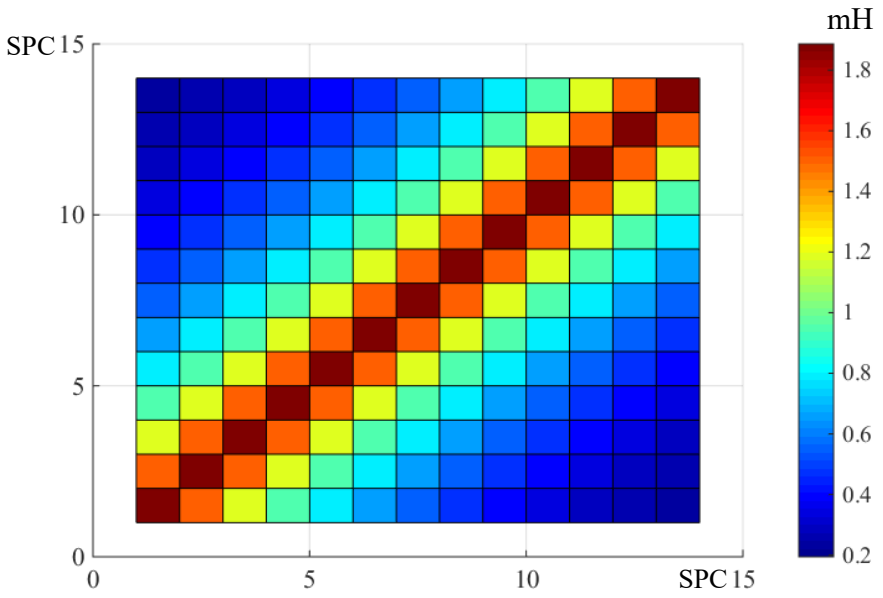

FIG. 6. The mutual inductances between different coils.

B. Distribution of the magnetization loss

Fig. 7 presents the variation of the magnetization loss power on the NI HTS coils SPC8 ~ SPC14 in the ramping process. It also shows a symmetric distribution with that of the lower half SPC7~SPC1. The magnetization loss power increases with the transport current from power supply. The power supply current stops increasing at t=40 s. The magnetization loss continues increasing and reaches the peak value at t=55 s, then drops slowly to zero. Both the flux density and flux variation rate determine the flux creep in superconducting layers, which induce the magnetization loss in superconducting layers. After t=40 s, the azimuthal current (also the flux density induced) continues increasing, as shown in Fig. 5(b); but the increase rate drops to zero

gradually. The comprehensive effects lead to a peak time difference between the magnetization loss power and power supply current (also the turn-to-turn loss power), which is at about 15 s in Fig. 7.

The results also show that the HTS coils on the ends of the magnet have much higher magnetization loss power W_{sc} than the coils in the middle part of the magnet. This distribution trend is opposite to that of the turn-to-turn loss power in Fig. 3. The total magnetization loss energy density Q_{sc} generated in the whole ramping process is shown in Fig. 8. The magnetization loss energy Q_{sc} shows a more significant non-uniform distribution among aligned coils than the turn-to-turn loss. Coils at ends (SPC1 and SPC14) generate about 43 % of the total magnetization loss energy on all the coils. In each NI HTS coil, take SPC 14 as an example, magnetization loss has more concentrations around three locations: middle part, inner and outer sides of the coil.

This non-uniform magnetization loss distribution can be explained by the magnetic field distribution in Fig. 9. In the ramping process, the coils at ends have much higher magnetic field perpendicular to the tape surface (B//c) than other coils. Due to the anisotropy of the tape's critical current, the coils on the ends of the magnet have lower critical current and therefore deeper flux penetration than others. On the other hand, the coils on the ends of the magnet are charged faster than others, therefore, its azimuthal current are always higher than that of other coils in the ramping process, as shown in Fig. 5. The higher real ramping rate of azimuthal current leads to faster flux variation, therefore higher magnetization loss power. Therefore, the coils on the ends of the magnet generate more magnetization loss. In each coil, take SPC14 as an example, the turns close to the inner and outer side of the coil have more flux penetration because of higher magnetic field parallel to the tape surface, therefore, more magnetization loss is generated on these turns, especially the turns on the inner side of the ending coils (SPC1 and SPC14). For the turns on the middle part of each coil, a higher perpendicular magnetic field can be seen, which leads to another magnetization loss energy density peak on these turns. Fig. 10 shows a normalized current density (J/J_c) in superconducting layers in the ramping process. The coils at the ends of the magnet (SPC1 and SPC14) have a larger penetration zone ($J \approx J_c$) than others. In each coil, the turns close to the inner side have more penetration zone than others. These agrees well with the magnetization loss energy density distribution in Fig. 8.

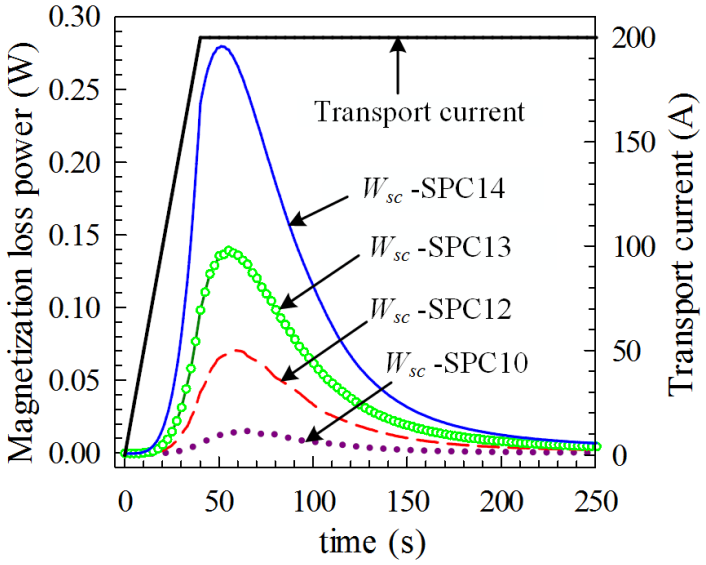

FIG. 7. The magnetization loss power on each NI SP coil in the ramping process.

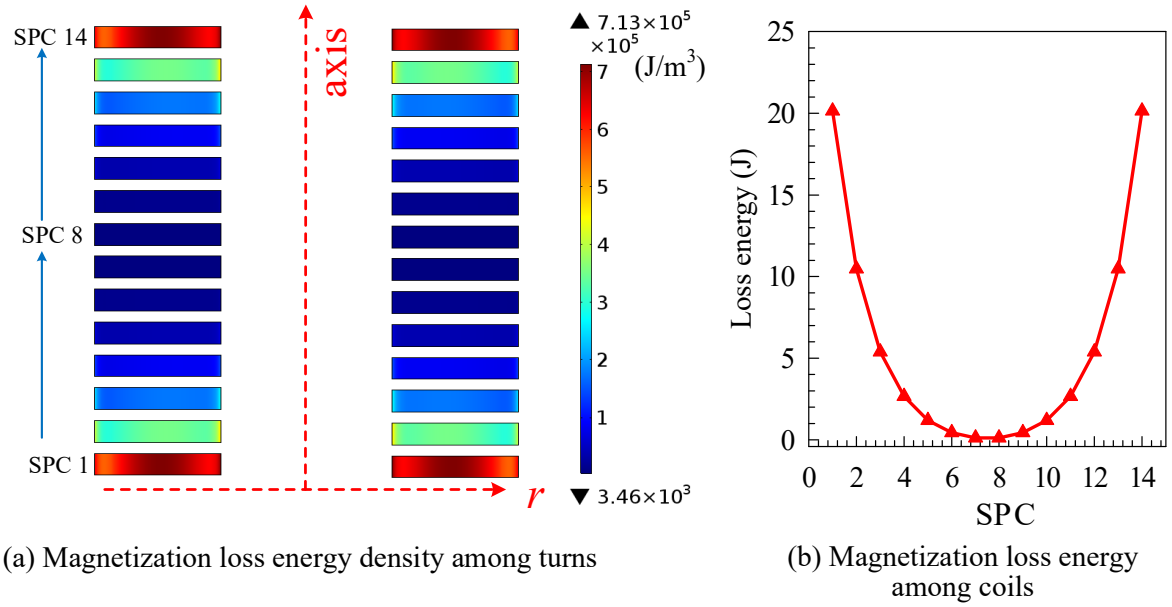

(a) Magnetization loss energy density among turns

(b) Magnetization loss energy among coils

FIG. 8. The distribution of NI REBCO coil's total magnetization loss energy in the whole ramping process, perfect cooling.

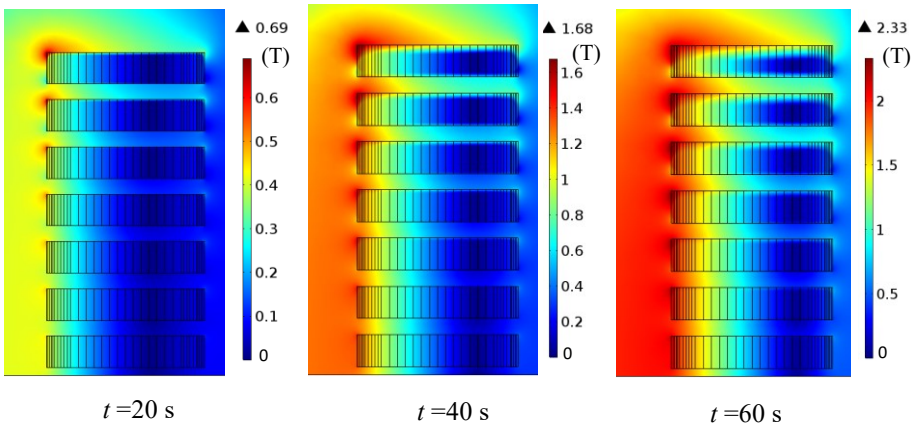

(a) Normal magnetic field, ||**B**||

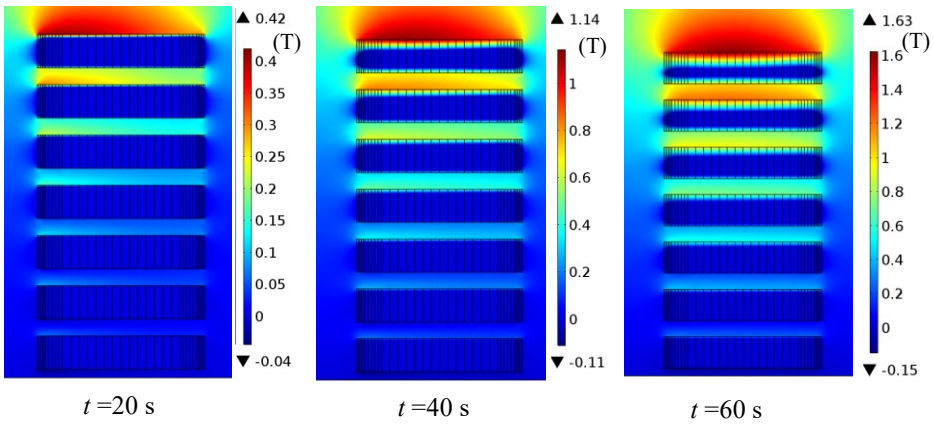

(b) Magnetic field perpendicular to the tape surface, B//c

FIG. 9. The magnetic field distribution of the magnet in the ramping process

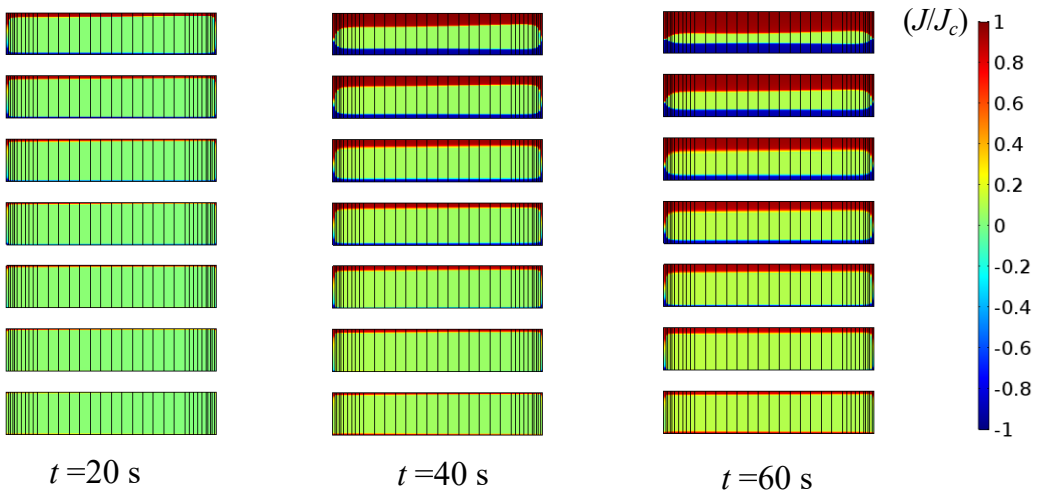

FIG. 10. The distribution of normalized current density (J/J_c) in superconducting layers in the ramping process.

C. Comparison with its insulated counterpart

To study the influence of the absence of turn-to-turn insulation on the ramping losses of the multiple REBCO coil system, simulations are performed on its insulated counterpart. This insulated magnet consists of 14 insulated SP REBCO coils which are the insulated counterparts of the above NI coils. The insulated magnet is ramped up to 200 A with a ramping rate of 5 A/s. No radial current is generated in the ramping process due to absolute electrical insulation between turns. Therefore, only magnetization loss in superconducting layers is induced. Fig. 11 shows the magnetization loss power W_{sc} in each insulated coil. It increases rapidly with the transport current from power supply, and reaches the peak point when the transport current stops increasing, then the magnetization loss drops to the ground fast. Compared to the results in Fig. 7, magnetization loss power of the insulated coils is much higher than that of the NI coils. In the insulated magnet, the azimuthal current in superconducting layers is always equal to the transport current from power supply. In the NI magnet, however, the ramping rate of azimuthal current is much lower than the transport current. With a same ramping rate of power supply, the NI magnet has a slower flux variation and therefore lower magnetization loss power W_{sc} in superconducting layers.

The results also show that, in the insulated magnet, highest magnetization loss power W_{sc} happens on the ends of the magnet (SPC14). This trend is similar with that in the NI magnet. Fig. 12 shows the magnetization loss energy Q_{sc} generated in the whole ramping process. The distribution of magnetization loss energy density Q_{sc} in NI magnet is approximately same with that in the INS magnet, though the loss powers W_{sc} are very different. The non-uniform distribution of magnetization loss in insulated magnet is also induced by the magnetic field distribution, which is same as that in the above NI magnet.

Figure 13 shows the total ramping losses in the coils of the NI and insulated HTS magnet. The total ramping losses energy of the NI magnet is much higher than that of its insulated counterpart with the same ramping rate of 5 A/s. In the insulted magnet, the coils at the ends generate more ramping losses energy than others, while in the NI magnet, the coils on the middle part generate more ramping losses than others because of major contribution from the turn-to-turn loss.

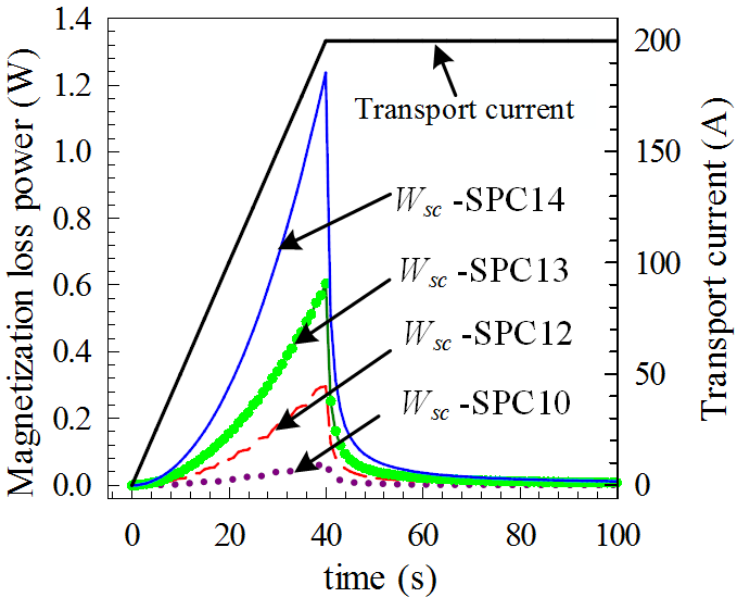

FIG. 11. The magnetization loss power on each INS SP coil in the ramping process.

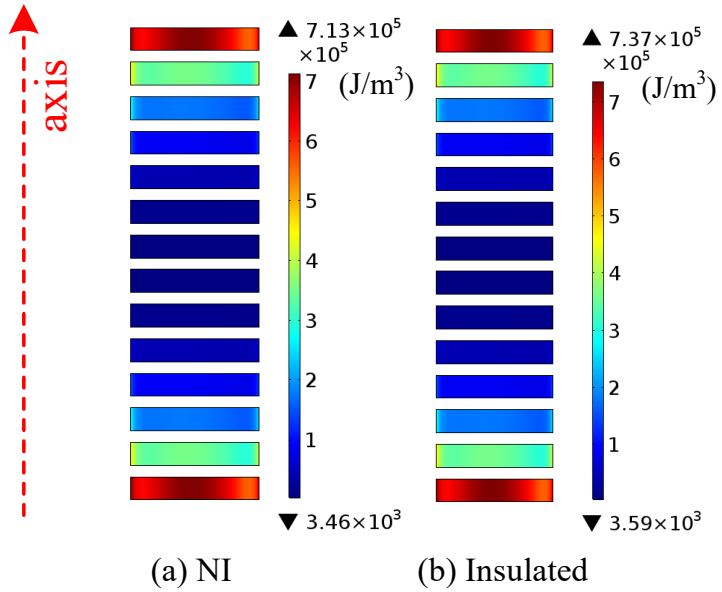

FIG. 12. Magnetization loss energy density among turns, NI coil VS INS coil

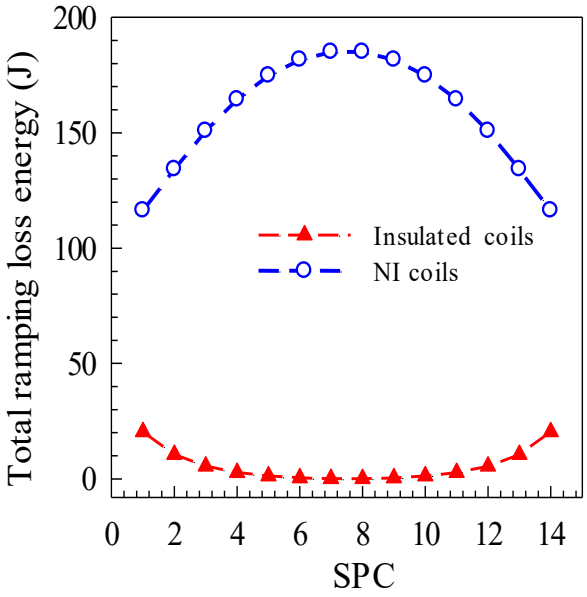

FIG. 13. The total ramping losses energy among coils in a multiple REBCO coil system, NI coil VS insulated coil.

D. Temperature rise induced by ramping losses

The above studies are based on perfect cooling condition, in which the cooling system is powerful enough to keep the coils at operating temperature 20 K. This section is to study the temperature rise induced by ramping losses under an adiabatic condition, in which the cooling power is zero. Here the equivalent turn-to-turn resistivity of the NI REBCO coils is assumed to be temperature independent. Fig. 14 shows the temperature changes in the NI coils induced by the ramping operation. The initial temperature is 20 K. Without cooling power, the turn-to-turn loss and magnetization loss can induce a considerable temperature rise (maximum value 23 K) on the NI coils in the ramping process. The NI coils on the middle part (SPC 7 and SPC 8) of the multiple coil system generate a higher temperature rise than other coils, due to the non-uniform ramping losses distribution among coils shown in Fig. 13. Towards the end of this ramping operation, the highest temperature on the middle coils (SPC1, SPC14) reaches 43 K; the temperature difference between middle SP coils (SPC 7, SPC 8) and end SP coils (SPC1, SPC14) reaches 5 K. Fig. 15 shows the ramping magnetization loss energy generated in the adiabatic and perfect cooling condition. Overall the adiabatic case seems to have very similar distribution pattern (qualitatively) to that of the perfect cooling case. Since the critical current of REBCO tapes drops with temperature rise, as shown in Eq. (2), more magnetization loss is generated when the perfect cooling condition is changed to adiabatic condition. The magnetization loss difference between two thermal conditions is show in Fig. 15(b). Here the increasing rate η is defined as:

$$\eta = \frac{Q_{adiabatic} - Q_{cooling}}{Q_{cooling}} \tag{7}$$

where $Q_{adiabatic}$ and $Q_{cooling}$ are the magnetization loss under adiabatic and perfect cooling condition respectively. The middle coils (SPC7, SPC8) show much more magnetization increases than the end coils (SPC1, SPC14). The magnetization loss of SPC7 and SPC8 increases 87 %, while that of SPC 1 and SPC 14 increases only 4 %. This is because the middle coils has larger temperature rise than the end coils, as shown in Fig. 13, which is about 5 K.

Note that the critical temperature of the magnet is 52 K with 200 A. Both the turn-to-turn loss and magnetization loss increase with the target current[19]. Quench may occur when the NI magnet is ramped to higher current (>200 A). Since the turn-

to-turn loss can be reduced by decreasing the ramping rate, higher operating current requires lower ramping rate and longer ramping time. Optimization and analysis on the ramping losses and cooling power is required for the practical NI REBCO magnets.

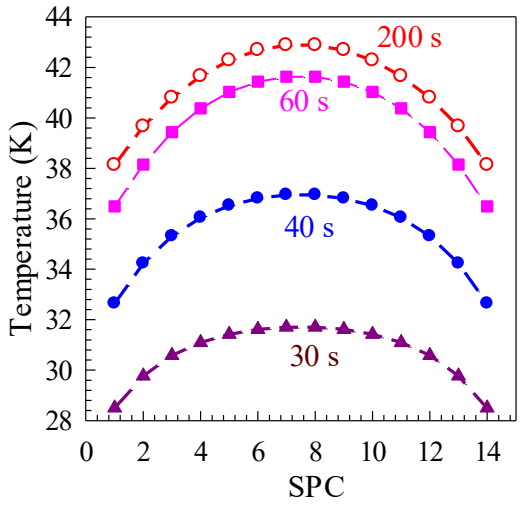

FIG. 14. The temperature distribution among SP NI coils and their thermal evolutions in the ramping process, ramping rate 5A/s adiabatic condition.

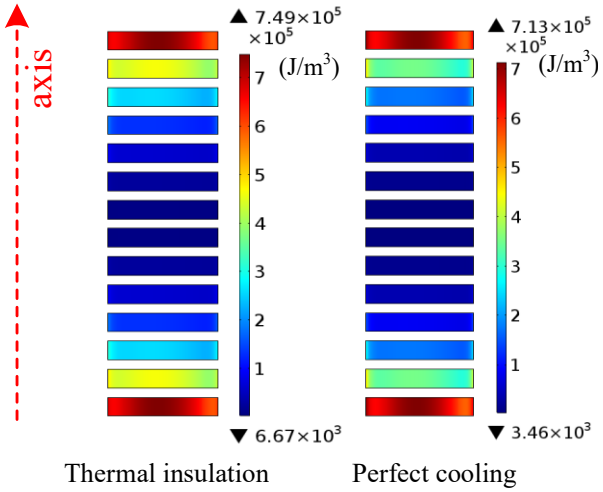

(a) Magnetization loss among turns

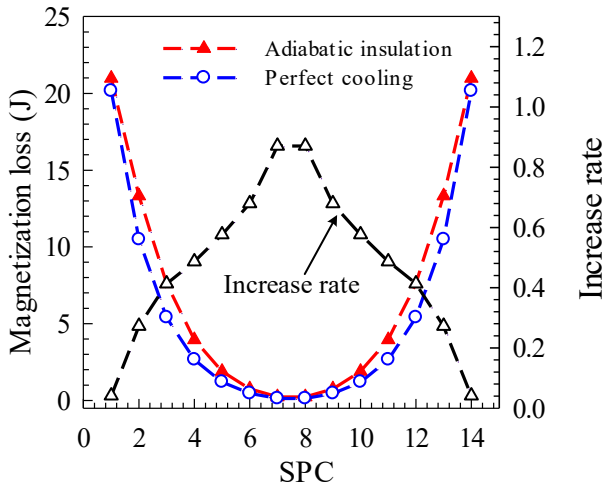

(b) Magnetization loss among NI coils and the relative increase rate

FIG. 15. Comparison on NI coils' magnetization loss during the ramping operation, adiabatic condition VS perfection cooling condition.

V. OPTIMIZATION ON THE RAMPING LOSSES DISTRIBUTION

The above studies show that the turn-to-turn loss generated in a ramping process shows a significant non-uniform distribution in a multiple NI REBCO coil system. It may induce a considerable non-uniform temperature rise on the coils. In a conventional insulated HTS magnets with multiple coils, the coils on magnet ends have a higher quench risk than others, due to higher perpendicular magnetic field and more ramping losses generated, as shown in Fig. 12. In the NI HTS magnets, the NI coils on the middle part of the multiple coil system generates more turn-to-turn loss and show a higher temperature rise during the ramping operations. Therefore, an additional quench risk happens on the middle coils, which needs more attentions. For a HTS magnet with multiple NI coils, measures are required to improve the ramping turn-to-turn loss distribution among coils, so that the local heat spot can be removed and the thermal stability of the HTS magnet can be enhanced.

In the above studies, the 14 identical SP NI coils have a same turn-to-turn resistivity, 70 $\mu\Omega\cdot cm^2$. In fact, the turn-to-turn resistivity of NI REBCO coils varies in a large range, 10~1000 $\mu\Omega\cdot cm^2$ [24, 46-49]. It mainly depends on winding tension, tape surface condition, materials of substrate and laminations, and impregnation technique [24, 25, 50, 51]. Therefore, it can be adjusted and maintained by controlling these parameters. It can be changed by adjusting winding tension, surface condition, substrate materials and so on. Since the turn-to-turn loss is generated by the radial current and turn-to-turn resistivity, its distribution should be optimized by adjusting turn-to-turn resistivity. Therefore, three other cases are designed, in which the 14 NI coils have a graded turn-to-turn resistivity. As shown in Fig. 16(a), Case 1 ~ Case 3 have a graded turn-to-turn resistivity among coils, Case 0 is the above situation with an identical turn-to-turn resistivity. All the other parameters of these coils are same with that in Table I. The magnets are ramped to 200A with a ramping rate of 5 A/S. Fig. 16(b) shows the distribution of turn-to-turn loss energy density among turns under the four cases. Fig. 17 shows the turn-to-turn loss among coils. The results show that a much more uniform turn-to-turn loss distribution is achieved in the multiple NI coil system by applying a graded turn-to-turn resistivity on the NI coils. However, in each NI coils, the turn-to-turn loss still shows a considerable non-uniform distribution among turns, as shown in Fig. 16(b). This can be improved by applying a graded turn-to-turn resistance on each turn of each SP NI coils.

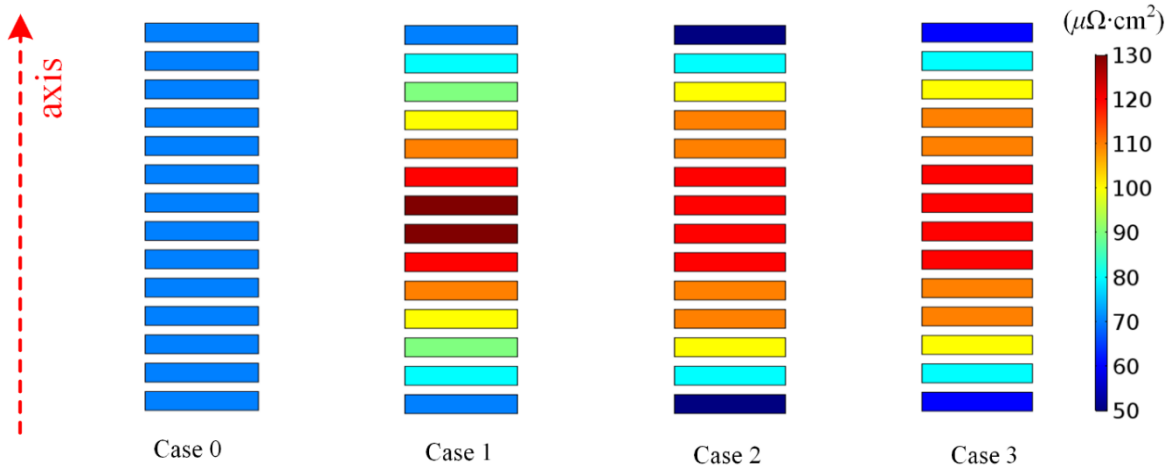

(a) Turn-to-turn resistivity ($\mu\Omega\cdot cm^2$)

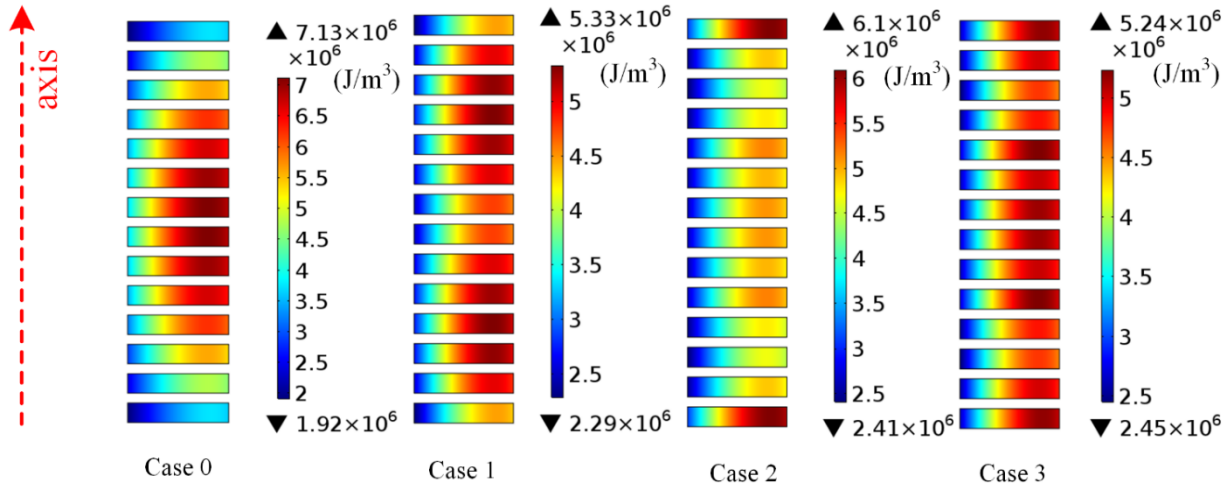

(b) Turn-to-turn loss energy density (J/m^3)

FIG. 16. The turn-to-turn loss energy density among turns, under 4 different grading turn-to-turn resistivity distribution. 4 cases of graded turn-to-turn resistivity have been demonstrated. Case 0 has the most non-uniform loss distribution, and case 1 and 2 are less optimized, and the case 4 is most optimized regarding the turn-to-turn loss.

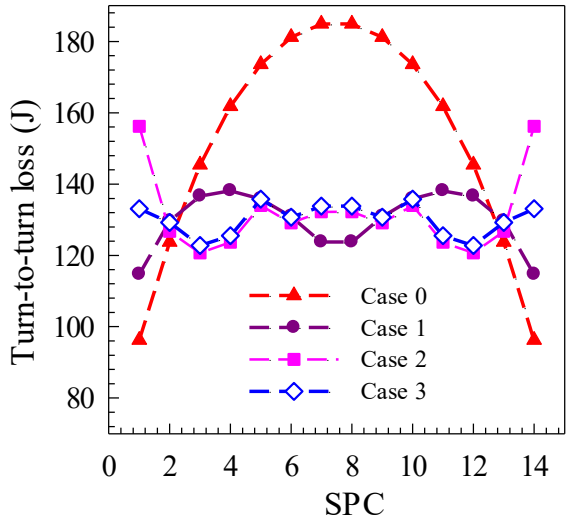

FIG. 17. The turn-to-turn loss energy among coils with 4 no grading and graded turn-to-turn resistivity approaches.

VI. CONCLUSIONS

This paper presents the ramping losses characteristics of a HTS magnet consisting of multiple NI coils. A hybrid numerical model has been developed and calculate the turn-to-turn ramping losses and magnetization loss inside all NI REBCO coils, which effectively couples the equivalent circuit network model, the electromagnetic model and the thermal model. The distribution of ramping losses along the turns and temperature rise among the coils have been summarized and analyzed, with the following primary findings:

First, in the HTS magnet with multiple NI coils, both the turn-to-turn loss and magnetization loss show a significant non-uniform distribution among coils. The highest turn-to-turn loss is generated on the middle coils of the magnet, while the highest magnetization loss is generated on the end coils of the magnet. The distribution of turn-to-turn loss is determined by electromagnetic coupling between coils. The distribution of magnetization loss is determined by magnetic field distribution, especial the field perpendicular to the tape surface. The turn-to-turn loss is one order of magnitude higher than the magnetization loss. The total ramping losses of the NI magnet shows a peak on the middle part of the magnet. Therefore, with the constant turn-to-turn resistivity, the ramping losses have intrinsic non-uniform distribution in the multiple NI HTS coils system.

With the embedded thermal model, it has been found that, the ramping losses, especially the turn-to-turn loss, lead into a significant temperature rise on the NI coils, and accordingly its non-uniform distribution among coils can result in a considerable temperature difference among coils. The middle coils (near mid-plane) of the multiple NI coil system have the highest temperature rise in the ramping process, though in a conventional insulated HTS magnet, the coils on the ends have a higher quench risk. It adds the extra quench risk on the magnet and requires more design analysis.

To solve the non-uniform loss distribution, the turn-to-turn resistivity has been adjusted to have a gradual changing pattern. Four cases of ramping losses have been calculate and compared with the four cases of turn-to-turn resistivity grading. With the optimized turn-to-turn resistivity grading on the multiple coils, a much more uniform turn-to-turn loss distribution among coils has been achieved. It is expected to enhance the thermal stability of the NI HTS magnet by optimizing the turn-to-turn resistivity of the NI coils.

Reference

1. S. Hahn, D. K. Park, J. Bascunan and Y. Iwasa, IEEE Appl. Supercond. **21** (3), 1592-1595 (2011).
2. A. V. Dudarev, A. V. Gavrilin, Y. A. Ilyin, V. E. Keilin, N. P. Kopeikin, V. I. Shcherbakov, I. O. Shugaev and V. V. Stepanov, in *Applied Superconductivity 1997, Vols 1 and 2: Vol 1: Small Scale and Electronic Applications; Vol 2: Large Scale and Power Applications*, edited by H. Rogalla and D. H. A. Blank (1997), pp. 1615-1618.
3. S. Choi, H. C. Jo, Y. J. Hwang, S. Hahn and T. K. Ko, IEEE Appl. Supercond. **22** (3) (2012).
4. H. Song, P. Brownsey, Y. Zhang, J. Waterman, T. Fukushima and D. Hazelton, IEEE Appl. Supercond. **23** (3), 4600806-4600806 (2013).
5. S. Hahn, Y. Kim, J. Song, J. Voccio, J. Ling, J. Bascunan and Y. Iwasa, IEEE Appl. Supercond. **24** (3) (2014).
6. Y. Iwasa and S. Hahn, Applied Physics Letters **103** (25) (2013).
7. S. Hahn, D. K. Park, J. Voccio, J. Bascunan and Y. Iwasa, IEEE Appl. Supercond. **22** (3) (2012).
8. W. Yawei, X. Deqiang, S. Hao, L. Xu, S. Jie, L. Ke, H. Zhiyong, J. Zhijian and L. Zhuyong, IEEE Appl. Supercond. **25** (3), 4600305 (2015).
9. S. Hahn, K. Radcliff, K. Kim, S. Kim, X. B. Hu, K. Kim, D. V. Abraimov and J. Jaroszynski, Supercond. Sci. Technol. 29 (10) (2016).
10. K. Kwangmin, G. Byeong-Soo, P. Minwon and Y. In-Keun, IEEE Appl. Supercond. **25** (3), 5203704 (5203704 pp.)-5203704 (5203704 pp.) (2015).
11. H. W. Weijers, W. D. Markiewicz, A. V. Gavrilin, A. J. Voran, Y. L. Viouchkov, S. R. Gundlach, P. D. Noyes, D. V. Abraimov, H. Bai, S. T. Hannahs and T. P. Murphy, IEEE Appl. Supercond. **26** (4), 1-7 (2016).
12. Y. Wang, C. Wan Kan and J. Schwartz, Supercond. Sci. Technol. **29** (4), 045007 (045011 pp.)-045007 (045011 pp.) (2016).
13. J. H. Liu, Y. M. Dai and L. K. Li, Cryogenics **79**, 79-84 (2016).
14. Z. Ang, I. Bejar, L. Bottura, D. Richter, M. Sheehan, L. Walckiers and R. Wolf, IEEE Appl. Supercond. **9** (2), 742-745 (1999).
15. A. R. Burgers and J. A. Eikelboom, IEEE Transactions on Magnetics **28** (1), 850-853 (1992).
16. J. Lu, E. S. Choi, H. Kandel, D. V. Abraimov and W. D. Markiewicz, IEEE Appl. Supercond. **24** (3) (2014).
17. W. Yuan, A. M. Campbell and T. A. Coombs, Supercond. Sci. Technol. **22** (7) (2009).
18. M. Zhang, W. Yuan, J. Kvitkovic and S. Pamidi, Supercond. Sci. Technol. **28** (11) (2015).
19. Y. Wang, H. Song, W. Yuan, Z. Jin and Z. Hong, J Appl Phys **121** (11) (2017).
20. H. De Gersem, S. Koch, S. Y. Shim, E. Fischer, G. Moritz and T. Weiland, IEEE Appl. Supercond. **18** (2), 1613-1616 (2008).
21. J. J. Rabbers, A. Dudarev, R. Pengo, C. Berriaud and H. H. J. ten Kate, IEEE Appl. Supercond.**16** (2), 549-552 (2006).
22. Y. Wang and H. Song, Supercond. Sci. Technol. **29** (7), 075006 (2016).
23. K. L. Kim, Y. H. Choi, D. G. Yang, J. B. Song and H. G. Lee, Supercond. Sci. Technol. **27** (1) (2014).
24. T. Lecrevisse and Y. Iwasa, IEEE Appl. Supercond. **26** (3) (2016).
25. T. S. Lee, Y. J. Hwang, J. Lee, W. S. Lee, J. Kim, S. H. Song, M. C. Ahn and T. K. Ko, Supercond. Sci. Technol. **27** (6) (2014).
26. K. Li, Y. Wang, P. Yang, C. Ma, D. Qiu, Y. Pan, Z. Li, Z. Jin and Z. Hong, IEEE Appl. Supercond. **27** (4), 1-5 (2017).
27. J. B. Song, S. Hahn, Y. Kim, D. Miyagi, J. Voccio, J. Bascunan, H. Lee and Y. Iwasa, IEEE Appl. Supercond. **25** (3) (2015).
28. Y. Wang, H. Song, D. Xu, Z. Y. Li, Z. Jin and Z. Hong, Supercond. Sci. Technol. **28** (4) (2015).
29. K. Seokho, H. Seungyong, K. Kwangmin and L. David, Supercond. Sci. Technol. **30** (3), 035020 (2017).
30. Z. Zhang, C. H. Kim, J. G. Kim, J. Kvitkovic, S. Pamidi, M. Zhang, J. Li and W. Yuan, Journal of Superconductivity and Novel Magnetism **30** (2), 387-393 (2017).
31. J.-B. Song, S. Hahn, T. Lecrevisse, J. Voccio, J. Bascunan and Y. Iwasa, Supercond. Sci. Technol. **28** (11) (2015).
32. S. Yoon, K. Cheon, H. Lee, S.-H. Moon, S.-Y. Kim, Y. Kim, S.-H. Park, K. Choi and G.-W. Hong, IEEE Appl. Supercond. **24** (3) (2014).
33. S. Yoon, J. Kim, H. Lee, S. Hahn and S. H. Moon, Supercond. Sci. Technol. **29** (4) (2016).
34. Y. Wang, P. Wang, K. Li, H. Song, J. Yang, C. Ma, Z. Jin and Z. Hong, IEEE Appl. Supercond. **27** (4), 3700105 (2017).
35. J. Bascunan, S. Hahn, T. Lecrevisse, J. B. Song, D. Miyagi and Y. Iwasa, IEEE Appl. Supercond. **26** (4) (2016).
36. T. Benkel, N. Richel, A. Badel, X. Chaud, T. Lecrevisse, F. Borgnolutti, P. Fazilleau, K. Takahashi, S. Awaji and P. Tixador, IEEE Appl. Supercond. **27** (4), 1-5 (2017).
37. K. R. Bhattarai, K. Kim, S. Kim, S. Lee and S. Hahn, IEEE Appl. Supercond. **PP** (99), 1-1 (2017).
38. J. H. Liu, Q. L. Wang, Y. M. Dai, L. K. Li and S. S. Song, IEEE Appl. Supercond. **27** (4) (2017).
39. T. Qu, P. C. Michael, J. Bascuñán, T. Lécrevisse, M. Guan, S. Hahn and Y. Iwasa, IEEE Appl. Supercond. **27** (4), 1-5 (2017).
40. K. Ibrahim, K. Matthew, I. Yury and W. Ulrich, Supercond. Sci. Technol. **30** (4), 04LT01 (2017).

41. H. Song and Y. Wang, IEEE Appl. Supercond. **26** (4), 1-1 (2016).
42. F. Grilli, F. Sirois, V. M. R. Zermeno and M. Vojenciak, IEEE Appl. Supercond. **24** (6) (2014).
43. C. Wan Kan, P. J. Masson, C. Luongo and J. Schwartz, IEEE Appl. Supercond. **20** (6), 2370-2380 (2010).
44. C. Wan Kan and J. Schwartz, IEEE Appl. Supercond. **21** (6), 3628-3634 (2011).
45. S. Noguchi, R. Itoh, S. Hahn and Y. Iwasa, IEEE Appl. Supercond. **24** (3) (2014).
46. W. D. Markiewicz, J. J. Jaroszynski, D. V. Abraimov, R. E. Joyner and A. Khan, Supercond. Sci. Technol. **29** (2), 25001-25001 (2016).
47. X. Wang, S. Hahn, Y. Kim, J. Bascunan, J. Voccio, H. Lee and Y. Iwasa, Supercond. Sci. Technol. **26** (3) (2013).
48. S. Noguchi, R. Miyao, K. Monma, H. Igarashi and A. Ishiyama, IEEE Appl. Supercond. **27** (4), 1-5 (2017).
49. L. Jun, G. Robert, H. Ke and H. Seungyong, Supercond. Sci. Technol. **30** (4), 045005 (2017).
50. K. L. Kim, S. Hahn, Y. Kim, D. G. Yang, J.-B. Song, J. Bascunan, H. Lee and Y. Iwasa, IEEE Appl. Supercond. **24** (3) (2014).
51. P. Heecheol, A. r. Kim, K. Seokho, P. Minwon, K. Kwangmin and P. Taejun, Physica C: Superconductivity and its Applications **504**, 138-143 (2014).